Postprint of the following paper: Wei,W.; Fu, S.*; Moan, T.; Lu, Z.; and Deng, S., (2017),“ A discrete-modules-based frequency domain hydroelasticity method for floating structures in inhomogeneous sea conditions”, Journal of Fluids and Structures, V.74, pp. 321-339.

Journal of Fluids and Structures, 2017, V.74, 321-339

A discrete-modules-based frequency domain hydroelasticity method for floating structures in inhomogeneous sea conditions

Wei Wei[a, b], Shixiao Fu[*a,b], Torgeir Moan[c], Ziqi Lu[a], Shi Deng[c]

[a] State Key Laboratory of Ocean Engineering, Shanghai Jiao Tong University, Shanghai, China

[b] Collaborative Innovation Centre for Advanced Ship and Deep-Sea Exploration, Shanghai, 200240, China;

[c] Norwegian University of Science and Technology, Trondheim, Norway

Abstract

Based on the three-dimensional (3D) potential theory and finite element method (FEM), this paper proposes a new numerical method for hydroelastic predictions of floating structures in inhomogeneous seabed and wave field conditions. The continuous floating structure is first discretized into rigid modules connected by elastic beams. The motion equations of the entire floating structure are established according to the six degrees of freedom (6DOF) motions of each module by coupling the hydrodynamics of the modules with the structural stiffness matrix of the elastic beams in the frequency domain. By applying different wave excitation forces onto different modules, this discrete-modules-based method then uniquely realizes application of various wave excitation forces onto different modules of the structures in inhomogeneous waves. The hydroelastic responses of a plate and a Wigley hull under an even and uneven seabed using the proposed method are verified against the results from the published model tests and the conventional 3D hydroelastic method. Finally, the effects of inhomogeneous waves on the distributions of the bending moment, shear force and vertical displacements of the freely floating plate are investigated. The results show that the inhomogeneity of waves may induce about 2~3 times increase of the force responses in a specific wave frequency.

Key words: Inhomogeneous wave field conditions; Stiffness matrix; Discrete-modules-based method; Hydroelastic responses; Wigley hull

[*] Corresponding author at: State Key Laboratory of Ocean Engineering, Shanghai Jiao Tong University, Shanghai, China.

E-mail address: shixiao.fu@sjtu.edu.cn (S. Fu).

1. Introduction

Since the late 1970s, hydroelasticity theory has been developed from 2D (Betts et al., 1977; Bishop et al., 1979) to 3D (Lee et al., 2015; Shin et al., 2015; Taghipour et al., 2009; Wu, 1984) and from linear (Bishop et al., 1986; Ohkusu and Namba, 2004) to nonlinear (Hu et al., 2012; Lee and Lee, 2016; Malenica and Tuitman, 2008; Wu et al., 1997). This theory has been widely applied in the design work of large-scale vessels and very large floating structures (VLFS') (Chen et al., 2006).

Two hydroelasticity approaches have been employed for the hydroelastic analysis of floating structures on an even seabed and in homogeneous wave conditions: the modal superposition method and direct method (Loukogeorgaki et al., 2012). Depending on the method used to obtain the structural modes, the modal superposition method can be further divided into the "dry" mode method (Senjanović et al., 2008a; Senjanović et al., 2008b) and the "wet" mode method (Humamoto and Fujita, 2002; Loukogeorgaki et al., 2012; Michailides et al., 2013). When it comes to the joining forces of the connectors of the interconnected floating structures, the local deflection/motion modes of the connectors have to first be calculated or predefined (Fu et al., 2007; Gao et al., 2011; Lee and Newman, 2000; Michailides et al., 2013; Newman, 2005), which sometimes becomes very hard or even impossible because of the strong coupling of the global deformation modes of the floating structures.

The direct method can analyze structures whose modes cannot be easily established using the full modes of the discretized system. Kim et al. (2007) and Yoon et al. (2014) combined the higher-order boundary element method (HOBEM) with the finite element method (FEM) and simplified the connectors as spring elements and plate finite elements, respectively, acquiring the hydroelastic responses of a multi-module VLFS and the joining forces in the connectors. Meanwhile, the direct method has been applied to the hydroelasticity of floating structures with liquid tanks by considering the couplings among structural motion, sloshing and waves (Lee et al., 2015).

The hydroelastic responses of floating structures in a uniform water depth were the main considerations in the above mentioned research. However, the effects of coastlines (Xia et al., 1999), seawalls (Ertekin and Kim, 1999) and varying sea bottom topographies (Utsunomiya et al.,

2001) on the hydroelastic responses of nearshore structures have been recognized as important issues in recent decades. Numerical methods for the hydroelastic responses of floating structures in variable bathymetry regions have been developed (Murai et al., 2003). Kyoung et al. (2005) investigated the effect of various sea-bottom topographies on the hydroelastic responses by adopting the FEM in a fluid domain. Song et al. (2005) used the boundary integral method of the finite water depth Green's function and the plate theory to analyze the vertical displacements of a VLFS model on an uneven sea bottom and verified that the uniform effect of the seabed should be considered in the hydroelastic analysis. Gerostathis et al. (2016) extended the coupled-mode model that was developed by Belibassakis and Athanassoulis (2005) to the hydroelasticity of structures with shallow drafts lying over variable bathymetry regions.

In addition to a complex seabed profile, the influences of the inhomogeneity of the incident waves (spatially varying incident wave angles and wave parameters) on the hydroelasticity have been considered during the design of large horizontal-scale structures near an island or in a fjord (Ding et al.; Lie et al., 2016).

Based on the recently developed method (Lu et al., 2016), a new numerical method is established for the prediction of the hydroelastic behaviors of floating structures in both homogeneous and inhomogeneous seabed and wave field conditions. This method is verified against the model tests and the conventional 3D hydroelastic method. The effects of the uneven sea bottom and the influences of inhomogeneous regular waves on the hydroelastic responses are investigated in numerical examples. The inhomogeneity of waves may induce a 30%~80% increase in the force responses, which should be considered in hydroelastic analyses.

2. Theoretical background

Fig. 1 provides an overview of the discrete-modules-based hydroelastic analysis process. The floating structure is first discretized into a set of rigid modules that are connected by elastic beams. Considering the hydrodynamic interactions between modules, the multi-body hydrodynamic theory is adopted to obtain the velocity potential of the flow field (the incident potential ϕ_I , the diffraction potential ϕ_D and the radiation potential ϕ_R) and the wave excitation force f_w, added mass A and damping coefficient C of various modules. The motions of each module are affected by the hydrodynamic interactions with the surrounding modules and are restricted by the displacement continuity of adjacent modules. The displacement continuity between modules is guaranteed by establishing an elastic beam with uniform section stiffness matrix $[k]$ between the equivalent centers of the modules. The displacements can be obtained by solving the coupled kinetic equation. Then, the bending moments, shear forces and torsional moments of the floating structure are determined based on the theory of structural mechanics.

No wet panels are set on the wall sides to avoid water resonance between two modules during the hydrodynamic calculation. Thus, the modules in the middle have two vertical walls, and those in the bow and stern have three. Simultaneously considering bending and torsional deformations in three-dimensional floating structures is difficult when adopting the simulation method of the beams. Therefore, the floating structure is discretized with only one module in the transverse direction for simplicity.

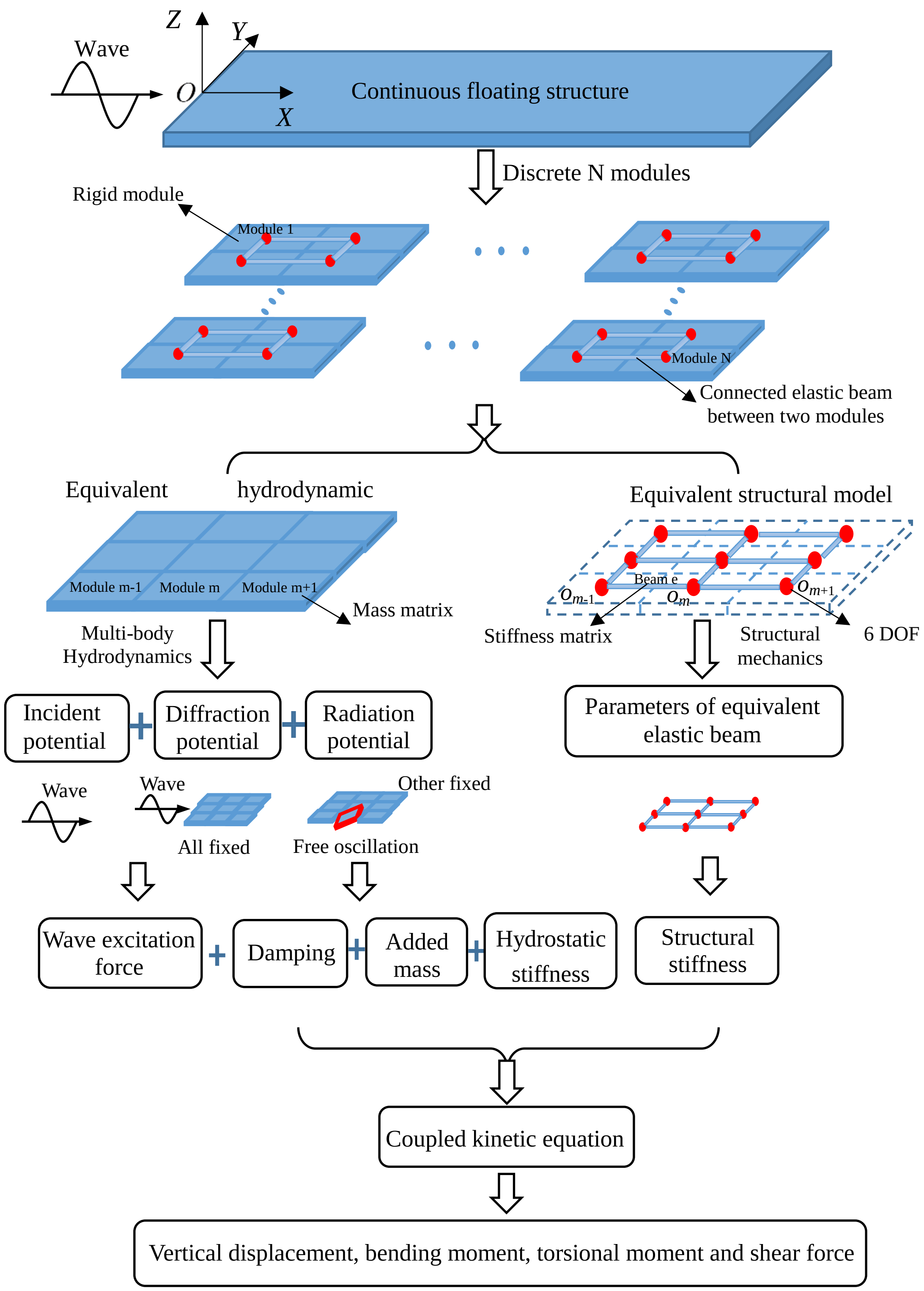

1

2 Fig. 1 Flow diagram of the numerical simulation

2.1. Hydrodynamic analysis

2.1.1. Coordinate system

The floating structure is only discretized in the longitudinal direction, so only one module is present in the transverse direction. Three right-handed coordinate systems are introduced to describe the wave-induced motion responses of a multi-module structure system: the global coordinate system *OXYZ*, body-fixed coordinate system $o_m x_m y_m z_m$ and reference coordinate system $o'_m x'_m y'_m z'_m$ ($m = 1, 2, ...N$). The global coordinate system (*OXYZ*) remains fixed in space, with *OXY* at the still water surface and the *Z* axis oriented straight up. The body-fixed coordinate system ($o_m x_m y_m z_m$) moves with the floating modules and is parallel to the coordinate axes of the global coordinate system ($OXYZ$) in its initial position. The reference coordinate system ($o'_m x'_m y'_m z'_m$) coincides with the body-fixed coordinate system ($o_m x_m y_m z_m$) in the initial stage and always remains at the balanced position. The incident wave angle is parallel with the *X* axis under an incident wave angle of $\theta = 0°$.

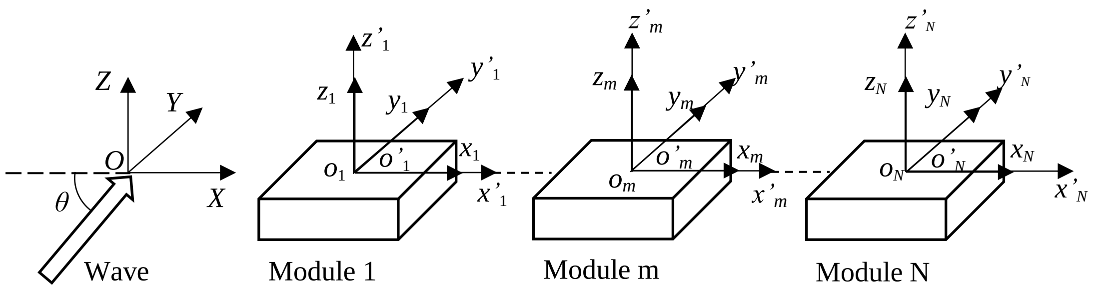

Fig. 2 Coordinate systems of a multi-body system

2.1.2. Governing equations and boundary conditions

The three-dimensional potential theory assumes that the fluid is ideal, incompressible, and irrotational, and the overall velocity potential in the global coordinate *OXYZ* is expressed as

$$\Phi(X,Y,Z,t) = \phi(X,Y,Z)e^{-i\omega t} \tag{1}$$

where ϕ refers to a time-independent space complex and ω is the circular frequency of the incident wave.

For a multi-module system, ϕ can be decomposed into

$$\phi = \phi_I + \phi_D + \sum_{m=1}^{N} \phi_R^{(m)} \tag{2}$$

where ϕ_I is the incident wave potential; ϕ_D is the diffraction potential; and $\phi_R^{(m)}$ denotes the radiation potential of module *m*, which can be expressed as

$$\phi_R^{(m)} = -i\omega \sum_{j=1}^{6} \xi_j^{(m)} \phi_{jR}^{(m)} \tag{3}$$

where $\phi_{jR}^{(m)}$ refers to the unit radiation velocity potential, in which module *m* oscillates in a unit velocity in the j^{th} direction with the other modules fixed, and $\xi_j^{(m)}$ refers to the complex motion amplitude of module *m* in the j^{th} mode.

In the global coordinate system *OXYZ*, the incident wave potential at a finite water depth can be expressed as

$$\phi_I = \frac{igA}{\omega} \frac{\cosh\left[k\left(Z+H\right)\right]}{\cosh kH} e^{ik(X\cos\theta + Y\sin\theta)} \tag{4}$$

where *A* refers to the incident wave amplitude; *H* is the water depth; *k* refers to the wave number; and *θ* is the wave direction, as illustrated in Fig. 2.

The radiation potential $\phi_{jR}^{(m)}$ of module *m* satisfies the governing equation and boundary conditions in the fluid domain Ω, including the linearized free-surface condition (S_F), body surface condition (S_n), sea bottom condition (S_B) and distant radiation condition (S_∞), as shown in Eq. (5). The simulated multi-module model has no wet panels on the wall sides between modules to avoid resonance in the gaps. Solving this model in mathematics is reasonable because the body surface boundary conditions are consistent with the actual situation.

$$\begin{cases} in \;\; \Omega : \nabla^2 \phi_{jR}^{(m)} = 0 \\ on \;\; S_F : -\omega^2 \phi_{jR}^{(m)} + g \left.\dfrac{\partial \phi_{jR}^{(m)}}{\partial z}\right|_{z=0} = 0 \\ on \;\; S_n : \dfrac{\partial \phi_{jR}^{(m)}}{\partial n^{(n)}} = \begin{cases} n_j^{(m)}, & m = n \\ 0, & m \neq n \end{cases} \\ on \;\; S_B : \left.\dfrac{\partial \phi_{jR}^{(m)}}{\partial n}\right|_{Z=-H} = 0 \\ on \;\; S_\infty : \lim\limits_{r\to\infty}\left(r^{1/2}\left(\dfrac{\partial \phi_{jR}^{(m)}}{\partial r} - ik\phi_{jR}^{(m)} \right)\right) = 0 \end{cases} \tag{5}$$

For the diffraction problem, we assume that all the modules are fixed in the domain, with an incident wave acting on them. Similar to the radiation potential, the diffraction potential ϕ_D satisfies the governing equation and boundary conditions in the fluid domain but with a different body boundary condition:

$$on\ \ S_0 : \frac{\partial \phi_D}{\partial n} = -\frac{\partial \phi_I}{\partial n} \ \ , \quad S_0 = \sum_{m=1}^{N} S_m \tag{6}$$

2.1.3. Hydrodynamic forces and coefficients

The diffraction and radiation potential are first determined based on the three-dimensional Green's function method. Applying the linearized Bernoulli equation, the dynamic fluid pressure that acts on the mean wetted surface can be obtained. Finally, by integrating the pressure along the mean wetted surface, the j^{th}-order wave excitation force of module *m* in the body-fixed coordinate system can be expressed as

$$F_{wj}^{(m)} = \iint_{S_m} p n_j^{(m)} ds = i\rho\omega e^{-i\omega t} \iint_{S_m} \left(\phi_I + \phi_D\right) n_j^{(m)} ds \tag{7}$$

The force can be decomposed into two components:

$$\begin{cases} F_{Kj}^{(m)} = i\rho\omega e^{-i\omega t} \iint_{S_m} \phi_I n_j^{(m)} ds \\ F_{Dj}^{(m)} = i\rho\omega e^{-i\omega t} \iint_{S_m} \phi_D n_j^{(m)} ds \end{cases} \tag{8}$$

where $F_{Kj}^{(m)}$ is the Froude-Krylov force and $F_{Dj}^{(m)}$ refers to the diffraction force.

The j^{th}-order radiation force of module *m* that is generated by the free oscillations in the k^{th} mode of module *n* in the body-fixed coordinate system can be expressed as

$$F_j^{(mn)} = \iint_{S_m} p n_j^{(m)} dS = \rho\omega^2 \xi_k^{(n)} e^{-i\omega t} \iint_{S_m} \phi_k^{(n)} n_j^{(m)} dS \tag{9}$$

If we substitute the body boundary condition of the radiation potential $\frac{\partial \phi_j^{(m)}}{\partial n} = n_j^{(m)}$ into the above formula, Eq. (9) can be written as

$$A_{kj}^{(mn)} + \frac{iC_{kj}^{(mn)}}{\omega} = \rho \iint_{S_m} \phi_k^{(n)} \frac{\partial \phi_j^{(m)}}{\partial n} dS \tag{10}$$

where the subscripts *k* and *j* denote the number of modes; the superscripts *m* and *n* are the number of modules; and $A_{kj}^{(mn)}$ and $C_{kj}^{(mn)}$ denote the added mass and damping coefficients in the j^{th} mode of module *m* from the module *n* oscillating in the k^{th} mode, respectively.

2.1.4. Hydrodynamic equations

The coupled motion equations of the floating multi-body system in the reference coordinate system can be expressed as follows based on Newton's Second Law of Motion:

$$\left(\begin{bmatrix} M^{(1)} & & \\ & \ddots & \\ & & M^{(N)} \end{bmatrix} + \begin{bmatrix} A^{(11)} & \cdots & A^{(1N)} \\ \vdots & \ddots & \vdots \\ A^{(N1)} & \cdots & A^{(NN)} \end{bmatrix}\right) \begin{Bmatrix} \ddot{x}^{(1)} \\ \vdots \\ \ddot{x}^{(N)} \end{Bmatrix} + \begin{bmatrix} C^{(11)} & \cdots & C^{(1N)} \\ \vdots & \ddots & \vdots \\ C^{(N1)} & \cdots & C^{(NN)} \end{bmatrix} \begin{Bmatrix} \dot{x}^{(1)} \\ \vdots \\ \dot{x}^{(N)} \end{Bmatrix} + \begin{bmatrix} K^{(1)} & & \\ & \ddots & \\ & & K^{(N)} \end{bmatrix} \begin{Bmatrix} x^{(1)} \\ \vdots \\ x^{(N)} \end{Bmatrix} = \begin{Bmatrix} F_w^{(1)} \\ \vdots \\ F_w^{(N)} \end{Bmatrix} \tag{11}$$

where $\left[M^{(N)}\right]$ refers to the 6×6 mass matrix of the N^{th} module; $\left[A^{(NN)}\right]$ and $\left[C^{(NN)}\right]$ are the added mass and damping coefficient matrices of module N, respectively, which can be derived from Eq. (10); $\left[K^{(N)}\right]$ is the 6×6 hydrostatic restoring coefficient matrix; $\left\{x^{(N)}\right\}$, $\left\{\dot{x}^{(N)}\right\}$ and $\left\{\ddot{x}^{(N)}\right\}$ are the rigid body displacement, velocity and acceleration arrays of module N, respectively, which are all 6×1 arrays; and $\left\{F_w^{(N)}\right\}$ is the wave excitation force array with 6 degrees, which can be derived from Eq. (7).

Eq. (11) can be simplified as

$$\left([M]+[A]\right)_{6N\times6N}\{\ddot{x}\}_{6N\times1}+[C]_{6N\times6N}\{\dot{x}\}_{6N\times1}+[K]_{6N\times6N}\{x\}_{6N\times1}=\{F_w\}_{6N\times1} \tag{12}$$

2.2. Structural analysis

According to the discrete-modules-based method, the motion of a single rigid module can be influenced by the hydrodynamic interactions from the other modules and restricted by the motion responses of the adjacent modules, ensuring the deformation continuity of the entire floating structure. Therefore, adjacent modules are connected with Euler-Bernoulli beams by considering St. Venant's torsion in the equivalent centers, as shown in Fig. 3. The structural stiffness matrix of elastic beams can be established based on structural mechanics and finite elements.

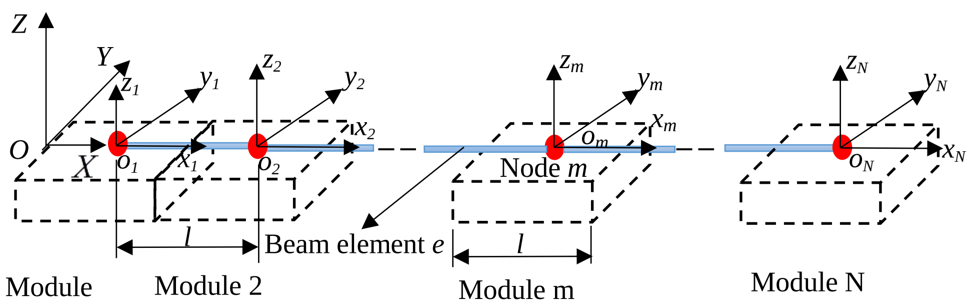

Fig. 3 Equivalent structural beam model, where l is the length of the equivalent beam between two modules.

2.2.1. Stiffness matrix

In the structural analysis, two coordinate systems, namely, the local coordinate system *mx'y'z'* and global coordinate system *OXYZ*, are selected to describe the deformation of the structure. Fig. 4 shows the two principal bending planes of the beam, namely, *x'mz'* and *x'my'*, with *x* as the beam axis and the origins in nodes *m* of element *e*.

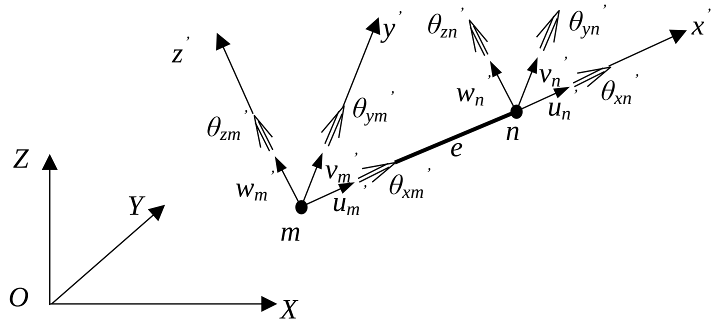

Fig. 4 Displacement of element *e*

The structural parameters of the equivalent beam element should correspond to those of a single rigid module to ensure deformation consistency with the continuous floating structure, which can be expressed as

$$\begin{cases} E \cdot b \cdot h = E_M A_M \\ E \cdot \dfrac{1}{12} b h^3 = E_M I_{My} \\ E \cdot \dfrac{1}{12} b^3 h = E_M I_{Mz} \\ G \beta b^3 h = G_M I_{M\rho} \\ G = \dfrac{E}{2(1+\mu)} \end{cases} \tag{13}$$

where $E_M A_M$, $E_M I_{My}$, $E_M I_{Mz}$, and $G_M I_M$ $G_M I_{M\rho}$ are the axial stiffness, vertical bending stiffness, transverse bending stiffness and torsional rigidity of a single module, respectively; E, G and μ are the elasticity modulus, shear modulus and Poisson's ratio of the equivalent beam, respectively; b and h are the rectangular width and breath of the cross section of the beam, respectively; and β is the torsional factor of a rectangular cross section, which is related to the ratio of h to b (Xia et al., 1998).

Then, the stiffness matrix $[k']^e$ of the beam element can be obtained in the local coordinate system:

$$
[k']^e = \begin{bmatrix}
\frac{EA}{l} & & & & & & & & & & & \\
0 & \frac{12EI_z}{l^3} & & & & & & & & & & \\
0 & 0 & \frac{12EI_y}{l^3} & & & & & & \textit{Symmetry} & & & \\
0 & 0 & 0 & \frac{GI_\rho}{l} & & & & & & & & \\
0 & 0 & \frac{-6EI_y}{l^2} & 0 & \frac{4EI_y}{l} & & & & & & & \\
0 & \frac{6EI_z}{l^2} & 0 & 0 & 0 & \frac{4EI_z}{l} & & & & & & \\
-\frac{EA}{l} & 0 & 0 & 0 & 0 & 0 & \frac{EA}{l} & & & & & \\
0 & \frac{-12EI_z}{l^3} & 0 & 0 & 0 & \frac{-6EI_z}{l^2} & 0 & \frac{12EJ_z}{l^3} & & & & \\
0 & 0 & \frac{-12EI_y}{l^3} & 0 & \frac{6EI_y}{l^2} & 0 & 0 & 0 & \frac{12EI_y}{l^3} & & & \\
0 & 0 & 0 & \frac{-GI_\rho}{l} & 0 & 0 & 0 & 0 & 0 & \frac{GI_\rho}{l} & & \\
0 & 0 & \frac{-6EI_y}{l^2} & 0 & \frac{2EI_y}{l} & 0 & 0 & 0 & 0 & 0 & \frac{4EI_y}{l} & \\
0 & \frac{6EI_z}{l^2} & 0 & 0 & 0 & \frac{2EI_z}{l} & 0 & \frac{-6EI_z}{l^2} & 0 & 0 & 0 & \frac{4EI_z}{l}
\end{bmatrix} \tag{14}
$$

where A is the area of the beam cross section, with $A=bh$, and I_y, I_z, and I_ρ are the vertical, horizontal and torsional inertia moments, respectively, with $I_y = \frac{1}{12}bh^3, I_z = \frac{1}{12}hb^3$ and $I_\rho = \beta b^3 h$.

The stiffness matrix in the local coordinate system $[k']^e$ can be transformed to the global coordinate system based on a small deformation assumption:

$$
[k]^e = \left[T^e\right]^T [k']^e \left[T^e\right] \tag{15}
$$

where $[k]^e$ is the element stiffness matrix of element e in the global coordinate system, $\left[T^e\right] = \begin{bmatrix} \lambda & & & \\ & \lambda & & \\ & & \lambda & \\ & & & \lambda \end{bmatrix}$ is the element variation matrix, and $[\lambda] = \begin{bmatrix} \cos(x'X) & \cos(x'Y) & \cos(x'Z) \\ \cos(y'X) & \cos(y'Y) & \cos(y'Z) \\ \cos(z'X) & \cos(z'Y) & \cos(z'Z) \end{bmatrix}$ is the direction cosine matrix of the local coordinate system that corresponds to the global coordinate system.

Then, the element stiffness matrix can be grouped in accordance with the nodes:

$$[k]^e = \begin{bmatrix} k_{mm}^e & k_{mn}^e \\ k_{nm}^e & k_{nn}^e \end{bmatrix} \tag{16}$$

where each sub-block $\left[k_{mn}^e\right]$ is a 6×6 matrix, and the nodes m and n of element e are the equivalent centers of module m and module m+1, respectively, in the multi-module system.

2.2.2. Deformation equation

Under external forces, the motion equation of the structure in the global coordinate system is as follows:

$$[m]\{\ddot{\delta}\} + [c]\{\dot{\delta}\} + [k]\{\delta\} = \{F\} \tag{17}$$

where $\{F\}$ refers to the external load vector in the global coordinate system; $[m]$ is the mass matrix of the beams; $[c]$ is the structural damping; $\{\delta\},\{\dot{\delta}\}$ and $\{\ddot{\delta}\}$ are the displacement, velocity and acceleration vectors, respectively; and $[k]$ denotes the stiffness matrix of the entire structure, which is overlaid with the above element stiffness matrix and can be expressed as follows:

$$[k] = \begin{bmatrix} k_{1,1}^1 & k_{1,2}^1 & & & & \\ k_{2,1}^1 & k_{2,2}^1 + k_{2,2}^2 & k_{2,3}^2 & & & \\ & k_{3,2}^2 & k_{3,3}^2 + k_{3,3}^3 & & & \\ & & & \cdot & & \\ & & & & \cdot & \\ & & & & & k_{N,N}^N \end{bmatrix} \tag{18}$$

2.3. Coupling equations of hydrodynamic and structure deformations

The structural damping is relatively negligible with respect to the hydrodynamic damping. Therefore, the forces on the beams in terms of waves and the structural attributions without the mass matrix of the beam itself and the structural damping after transforming the forces in the local coordinate system to the global coordinate system are shown in Fig. 5.

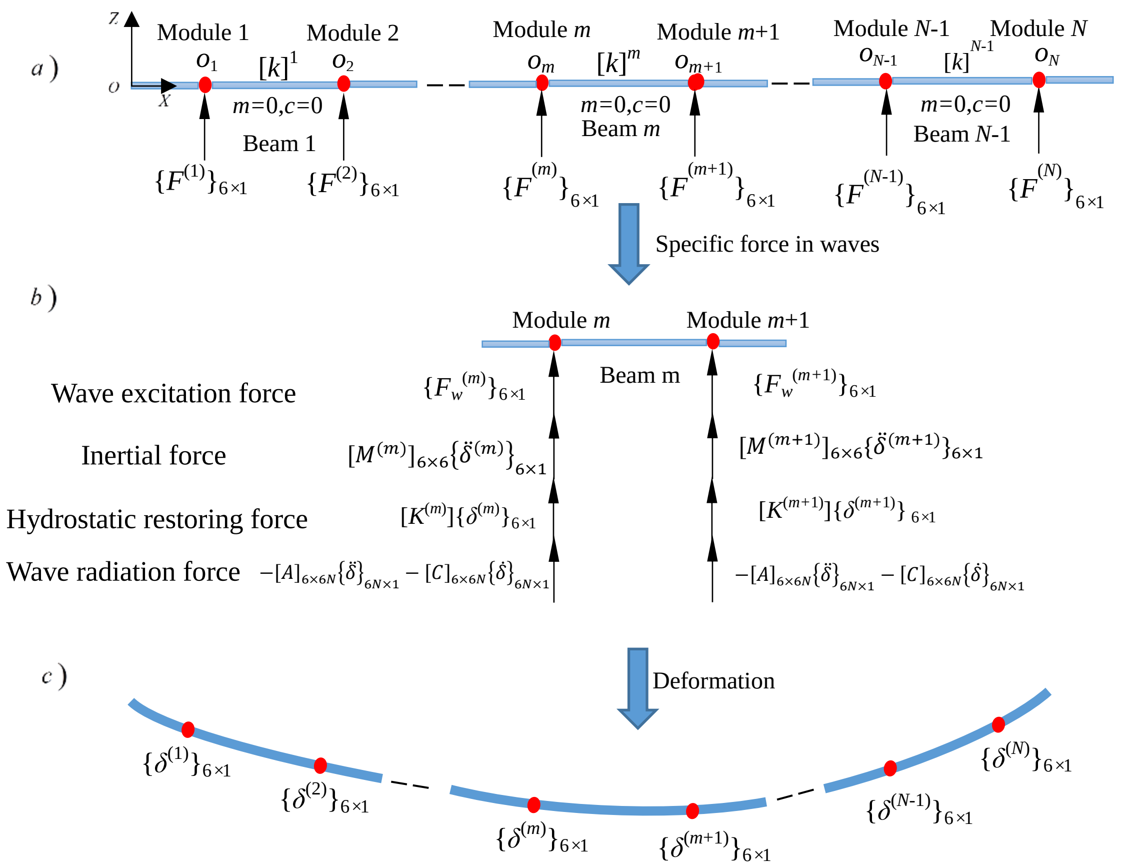

Fig. 5 Numerical method of the motion equation

After coupling the hydrodynamic parameters with the structural deformation equation in accordance with the numerical method of Fig. 1 for a floating system with N modules, the motion equations of the waves can be written as

$$\begin{bmatrix} k_{1,1}^{1} & & & & \\ & \cdot & & & \\ & & k_{m,m}^{m-1}+k_{m,m}^{m} & k_{m,m+1}^{m} & \\ & & k_{m+1,m}^{m} & k_{m+1,m+1}^{m}+k_{m+1,m+1}^{m+1} & \\ & & & & \cdot & \\ & & & & & k_{N,N}^{N} \end{bmatrix} \begin{Bmatrix} \delta^{(1)} \\ \cdot \\ \delta^{(m)} \\ \delta^{(m+1)} \\ \cdot \\ \delta^{(N)} \end{Bmatrix} = \begin{Bmatrix} F^{(1)} \\ \cdot \\ F^{(m)} \\ F^{(m+1)} \\ \cdot \\ F^{(N)} \end{Bmatrix} \tag{19}$$

where $\left[k_{m,m}^{m}\right]$ is the structural stiffness sub-matrix of the connection between module m and module m+1, as shown in Eq. (14) and Eq. (16); $\left\{\delta^{(m)}\right\}$ is the displacement vector of module m; and $\left\{F^{(m)}\right\}$ is the external force vector of module m and is related to the displacement $\{\delta\}$.

Based on the potential theory and shown in Fig. 5, $\{F\}$ includes the wave excitation force $\{F_w\}$, hydrostatic restoring force $[K]\{\delta\}$, inertial force $[M]\{\ddot{\delta}\}$ and wave radiation force, which contains two components: the added mass force $[A]\{\ddot{\delta}\}$ and damping force $[C]\{\dot{\delta}\}$.

In the above equation, we assume that $\{\delta\}$ and $\{F_w\}$ vary periodically with the stable frequency ω, which can be rewritten as

$$\{\delta\}=\{u\}e^{-i\omega t},\quad \{F_w\}=\{f_w\}e^{-i\omega t} \tag{20}$$

where $\{u\}$ and $\{f_w\}$ are the complex amplitudes of the displacement and wave excitation force vectors, respectively.

Consequently, Eq. (19) can be rewritten by separating the time variable:

$$\left(-\omega^2\left([M+A]_{6N\times 6N}\right)-i\omega[C]_{6N\times 6N}+[K+k]_{6N\times 6N}\right)\{u\}_{6N\times 1}=\{f_w\}_{6N\times 1} \tag{21}$$

where $[A]$, $[C]$ and $[K]$ are the added mass, damping and hydrostatic restoring coefficient matrices, respectively, which can be obtained from Eq. (12), and $\{u\}$ refers to the time-independent displacement vector.

The motion equation for a multi-module floating structure with connectors can be rewritten as

$$\begin{bmatrix} k_{1,1}^{1} & & & & & & \\ & . & & & & & \\ & & k_{m,m}^{m-1}+k_{m,m}^{m} & k_{m,l}^{m} & & & \\ & & k_{l,m}^{m} & k_{l,l}^{m}+k_{l,l}^{rot} & k_{l,r}^{rot} & & \\ & & & k_{r,l}^{rot} & k_{r,r}^{rot}+k_{r,r}^{m+1} & k_{r,m+1}^{m+1} & \\ & & & & k_{m+1,r}^{m+1} & k_{m+1,m+1}^{m+1} & \\ & & & & & & k_{N,N}^{N} \end{bmatrix}\begin{Bmatrix} \delta^{(1)} \\ . \\ \delta^{(m)} \\ \delta^{(l)} \\ \delta^{(r)} \\ \delta^{(m+1)} \\ . \\ \delta^{(N)} \end{Bmatrix}=\begin{Bmatrix} F^{(1)} \\ . \\ F^{(m)} \\ 0 \\ 0 \\ F^{(m+1)} \\ . \\ F^{(N)} \end{Bmatrix} \tag{22}$$

where $\left[k^{rot}\right]$ is the stiffness value of the connectors, which equals zero for a hinged connector, and $\left\{\delta^{(l)}\right\}$ and $\left\{\delta^{(r)}\right\}$ are the displacement vectors of the two nodes of the connector, which have the same translational displacement, as listed in Fig. 6.

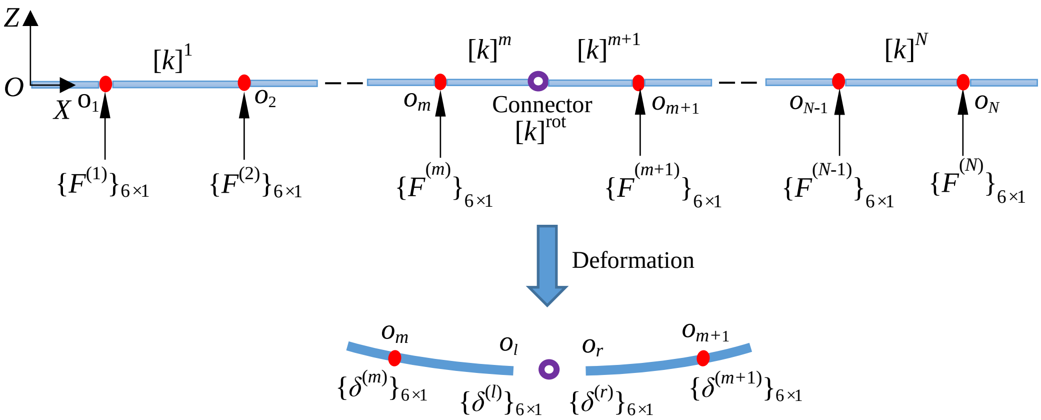

Fig. 6 Expression of the connector

2.4. Bending moments and shear forces

Structural bending moments and shear forces can be obtained by applying the beam bending theory. The motion equation in the frequency domain of Eq. (21) can be rewritten as

$$[k]_{6N\times 6N}\{u\}_{6N\times 1}=\{f_w\}_{6N\times 1}-\left(-\omega^2\left([M]_{6N\times 6N}+[A]_{6N\times 6N}\right)-i\omega[C]_{6N\times 6N}+[K]_{6N\times 6N}\right)\{u\}_{6N\times 1} \quad (23)$$

The forces on the right side of Eq. (23) can be considered the equivalent external loads $\{f\}$, and then Eq. (23) can be transformed into the basic equation of the FEM method:

$$[k]_{6N\times 6N}\{u\}_{6N\times 1}=\{f\}_{6N\times 1} \quad (24)$$

Finally, the problem is converted to solve the deformations and section forces of a free beam under concentrated forces, as shown in Fig. 7.

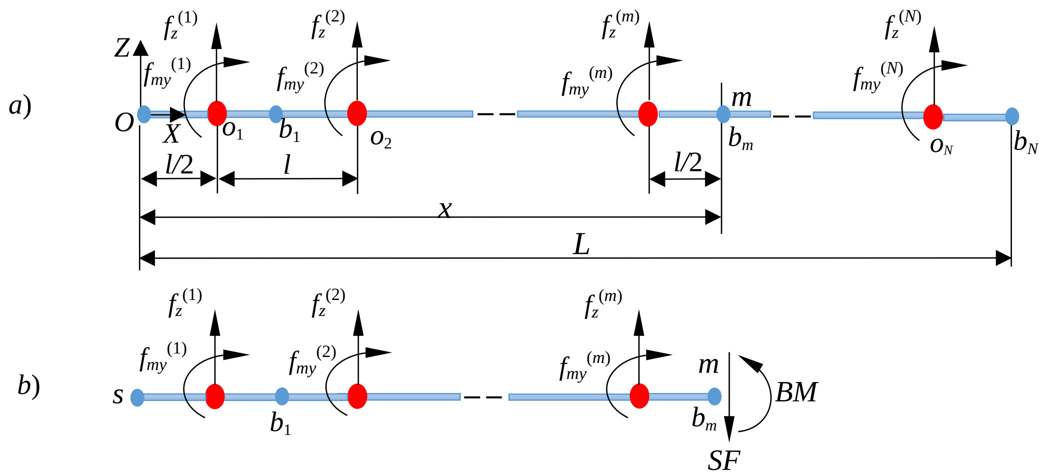

Fig. 7 External forces on the structure in the plane *xoz*, where $f_z^{(m)}$ and $f_{my}^{(m)}$ are the external

vertical force and moment of module m, respectively.

In Fig. 7(b), the bending moment and shear force at the discrete points (b_m) on the beam can be expressed as follows based on the beam bending theory:

$$\begin{cases} SF = \sum_{m} f_z^{(m)} \\ BM = \sum_{m} \left(f_{my}^{(m)} + f_z^{(m)} \cdot \left(x - \left(m - \frac{1}{2} \right) \cdot l \right) \right) \end{cases} \tag{25}$$

where BM and SF are the vertical bending moment and shear force in the beam cross section, respectively.

Similarly, the torsional moment can be obtained as follows:

$$T = \sum_{m} f_{mx}^{m} \tag{26}$$

For a multi-module structure with connectors, the forces on the connectors can be obtained by solving the section forces on the connection points by the same method as above.

2.5. Excitation forces in inhomogeneous waves

The continuous structure is first discretized into rigid modules with elastic beam connections based on the discrete module-based method, and then these modules are further grouped into different regions (including several modules) according to wave variations (different incident wave directions, heights and periods). The wave in each region is then assumed to be homogeneous as a normal uniform wave, as illustrated in Fig. 8.

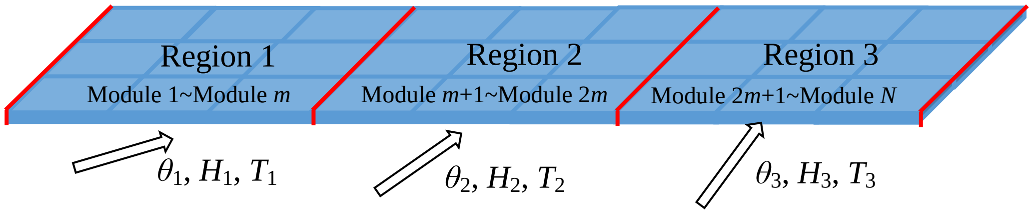

Fig. 8 Description of the inhomogeneous wave conditions

The inhomogeneity of the waves does not affect the radiations of the modules but introduces different wave excitations from incident and diffraction waves, which are always kept constant with one module (or the entire floating structure for conventional ships and platform structures). Under these circumstances, the j^{th}-mode wave excitation force on the n^{th} module within the k^{th} region could be written as follows:

$$f_{wj}^{(n)} = \frac{H_k}{2}\bar{f}_{wj}^{(n)}\left(\omega_k,\theta_k\right)\left(\cos\left(\beta_j^{(n)}\left(\omega_k,\theta_k\right)\right) - i\sin\left(\beta_j^{(n)}\left(\omega_k,\theta_k\right)\right)\right) \tag{27}$$

where the superscript n denotes the n^{th} module; k denotes the k^{th} region; j denotes the j^{th}-mode wave excitation force (j=1,...,6); H_k, ω_k and θ_k are the incident wave height, wave frequency and wave angle in the k^{th} region, respectively; $f_{wj}^{(n)}$ represents the j^{th}-DOF wave excitation force on the n^{th} module, whose position within the region is allocated according to its coordinates; $\bar{f}_{wj}^{(n)}\left(\omega_k,\theta_k\right)$ is the amplitude of $f_{wj}^{(n)}$; and $\beta_j^{(n)}\left(\omega_k,\theta_k\right)$ is the position-related phase angle of the wave excitation force on the n^{th} module in the j^{th} mode at a wave frequency of ω_k in the wave direction θ_k.

Consequently, the wave excitation forces on the discrete modules in the inhomogeneous wave on the right side of Eq. (21) can be expressed as

$$\left\{f_w\right\} = \left\{\left\{f_{w1}^{(1)}\right\},\ldots,\left\{f_{w1}^{(n)}\right\},\ldots,\left\{f_{w6}^{(n)}\right\},\ldots,\left\{f_{w6}^{(M)}\right\}\right\}^T \tag{28}$$

If we replace the right side of Eq. (21) with Eq. (28), we can finally obtain the hydroelastic-motion equations of the entire structure under inhomogeneous waves.

3. Validation of the proposed method in homogeneous conditions

3.1. Numerical model

The applicability and accuracy of the proposed method is verified by the hydroelastic responses of two models: a continuous floating plate (Fu et al., 2007) and a mathematical Wigley hull model that is formulated from Eq. (29). The parameters of the two models are listed in Table 1.

$$\begin{gathered}\eta = \left(1-\xi^2\right)\left(1-\zeta^2\right)\left(1+0.2\xi^2\right)+\zeta^2\left(1-\zeta^8\right)\left(1-\xi^2\right)^4 \\ \xi = \frac{2x}{L}, \eta = \frac{2y}{B}, \zeta = \frac{z}{d}\end{gathered} \tag{29}$$

in which L, B and d are the length, breadth and draft of the Wigley hull, respectively; $-L/2 \le x \le L/2$, $-B/2 \le y \le B/2$, $-d \le z \le 0$.

Table 1 Main parameters of the numerical model

Designation	Model 1 (Fu et al, 2007)	Model 2 (Journée, 1992)

Length, L (m)	300	300
Breadth, B (m)	60	45
Depth, D (m)	2	25
Draft, d (m)	0.5	18.75
Vertical Bending Stiffness, EI_y (N.m^2)	4.77E11	2.47E12 (mid-ship section)
Water Depth, H (m)	58.5	infinite

Both models are discretized into rigid modules that are connected by beams based on the proposed discrete-modules-based method. The characteristics of the elastic beams are listed in Table 2.

Table 2 Main parameters of the connecting elastic beams between the modules

Designation	Model 1	Model 2 (midship section)
Length, L(m)	37.5	15
I_y (m^4)	40	209.87
I_z (m^4)	3.6E4	839.5
J_x (m^4)	159.44	639.78
A	120	70.97

3.2. Verification results

The hydroelastic vertical displacements from the proposed method are compared to the experimental data by Yago and Endo (1996), and the distributions of the bending moments are compared to those from the three-dimensional hydroelasticity calculated by Fu et al. (2007). According to the recommendations in hydrodynamic analysis, at least four panels should be arranged within one wavelength. Thus, the required module number depends on the shortest wavelength of interest. In this paper, the model (Model 1 in Table 1) is discretized into 4, 8 and 15 modules for a convergence study.

Fig.9 shows the distribution of the vertical displacement and bending moment along the longitudinal direction of the structure for a 0° wave direction. The structural displacement and bending moment from the 8-module model match the test results and the predictions of the 3D hydroelastic method, while the results of the 4-module model do not show adequate accuracy. Compared to the results of the 15-module model, the 8-module model proves to be sufficiently accurate and more efficient. Fig. 10 illustrates the comparisons for different wavelengths and angles, and good agreements are observed.

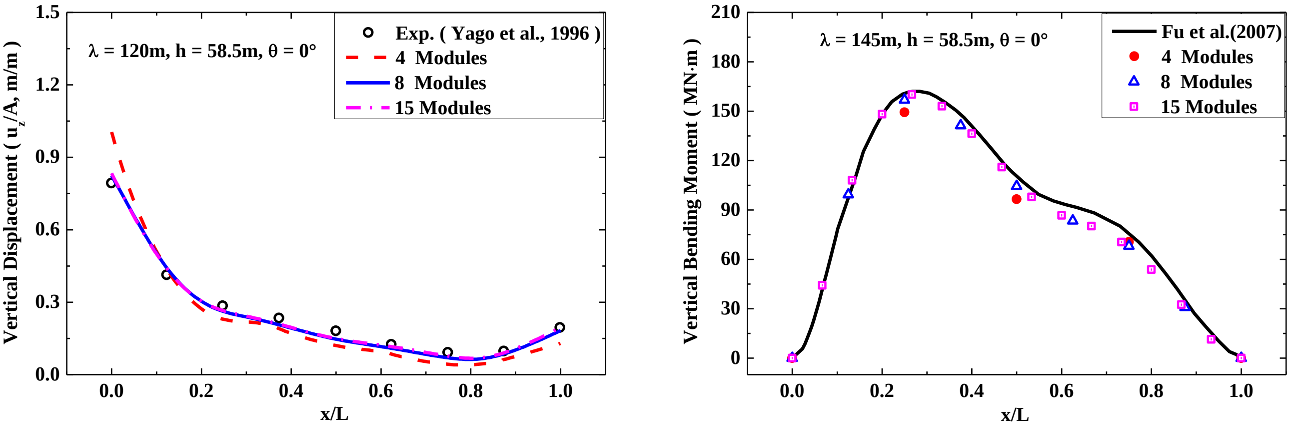

(a) Vertical displacement (b) Vertical bending moment

Fig.9 Vertical displacement and bending moment along the centerline of a continuous VLFS, with the effect from the number of modules.

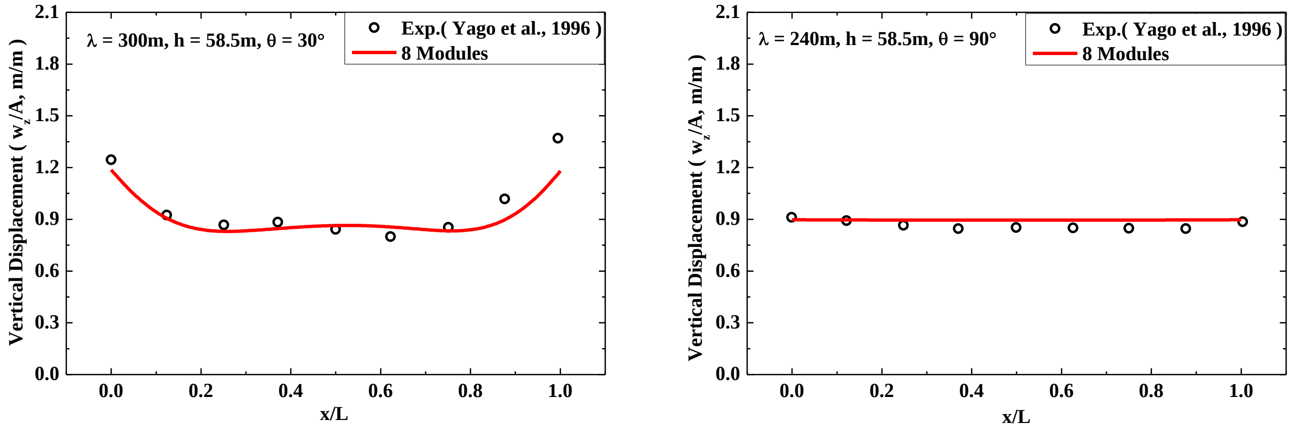

(a) Vertical displacement (b) Vertical displacement

Fig. 10 Vertical displacement along the centerline of a continuous VLFS for different wavelengths and angles.

Fig. 11 shows the torsional angle and moment from both the proposed method and the 3D hydroelastic method for a wave direction of 30°; good agreement is observed between the two results.

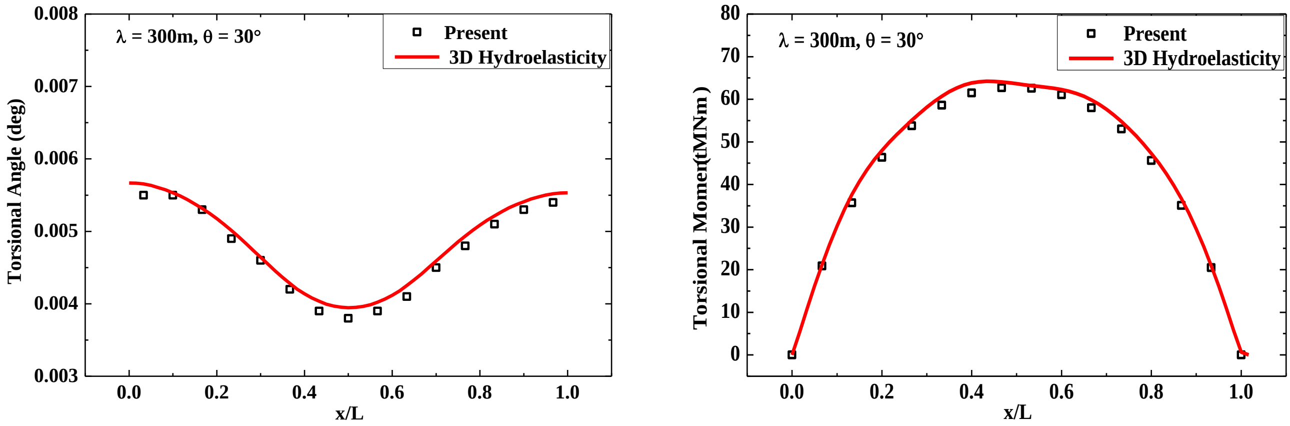

(a) Torsional angle (b) Torsional moment

Fig. 11 Torsional responses for a wave direction of 30 °

Fu et al. (2007) investigated the hydroelastic responses of an interconnected flexible floating structure by dividing a continuous VLFS into two substructures that are connected by a line connection. The proposed method can also simulate this type of hinged connector by "hinging" the two corresponding nodes, as shown in Fig. 12. In accordance with Fig. 13(a), the vertical displacements at the hinge joint from the proposed method are consistent with those by Fu et al. (2007). However, obtaining the connecting forces inside the hinges through the conventional modal superposition hydroelasticity theory is impossible. The calculations of the connecting forces inside the connectors can be directly solved by applying the proposed method, as illustrated in Fig. 13(b), where the shear force at the connector is plotted as a function of the incident wave frequency.

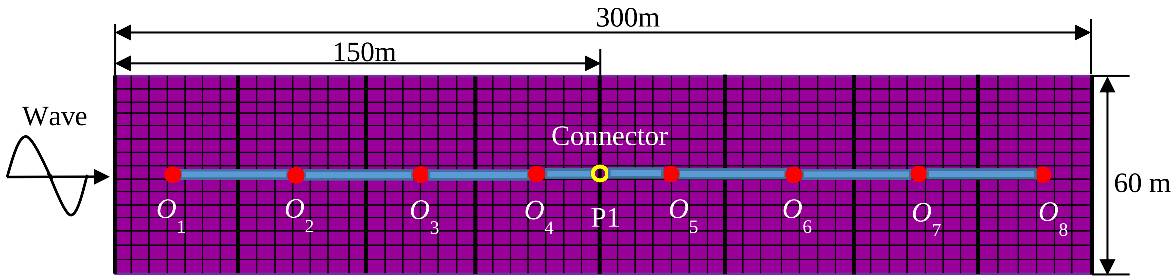

Fig. 12 Schematic plane view of an interconnected VLFS and equivalent beam model

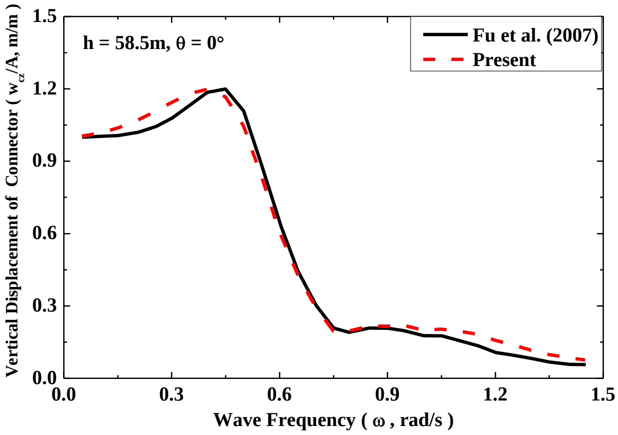

(a) Vertical displacement at the connector

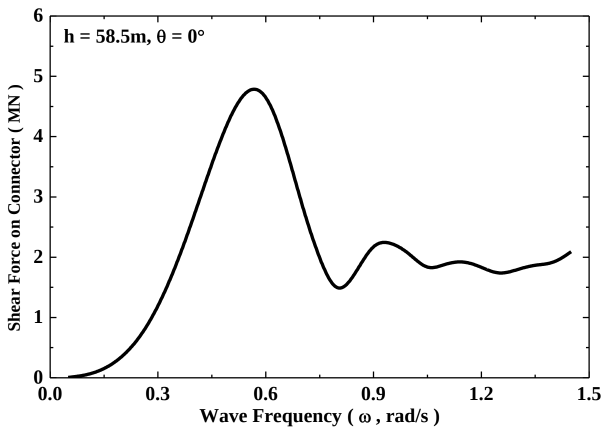

(b) Shear force on the connector

Fig. 13 Responses of the connector

Moreover, the hydroelastic responses of a Wigley hull model are investigated by both the proposed and 3D hydroelastic method to demonstrate the applicability of the method to ship-shaped structures. The Wigley model is discretized into 20 modules along the longitudinal direction after the convergence study. Fig. 14 provides the finite element model and the equivalent beam model with variable cross-sections of the Wigley hull. Table 3 lists only the parameters of the first 10 beam elements because of symmetry. Fig. 15 shows good agreement between the two methods, which indicates the applicability of the proposed method for the analysis of hydroelastic responses of ship-shaped structures.

Table 3 Parameters of the Wigley model

Module	b (m)	h (m)	Module	b (m)	h (m)
Module 1	0.823	0.411	Module 2	0.874	0.437
Module 3	0.926	0.463	Module 4	0.971	0.485
Module 5	1.013	0.507	Module 6	1.065	0.533
Module 7	1.110	0.555	Module 8	1.115	0.573
Module 9	1.191	0.596	Module 10	1.217	0.609

b and h are the width and height of the cross section of the equivalent beam, respectively.

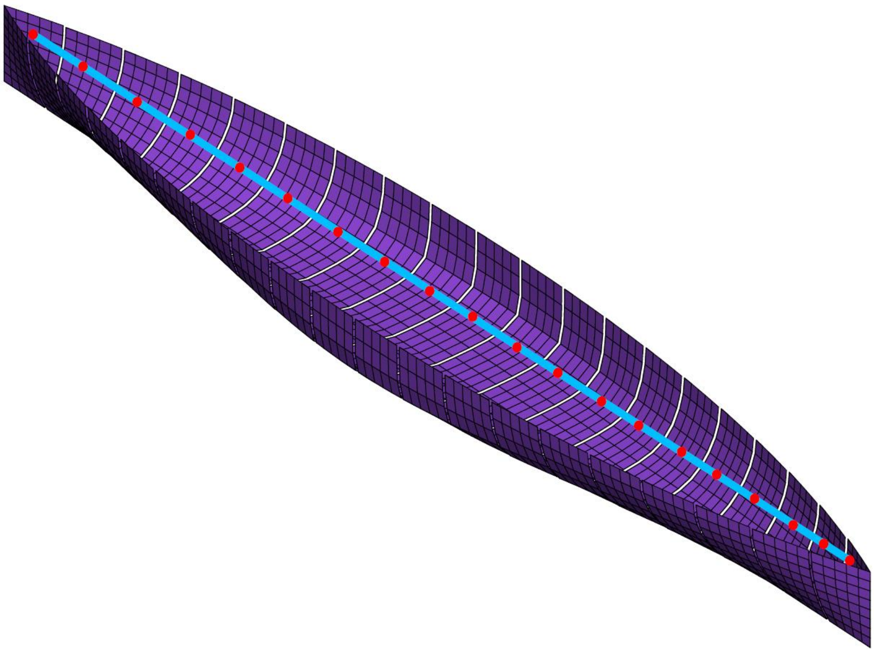

Fig. 14 FEM mode of the Wigley model and the equivalent beam model

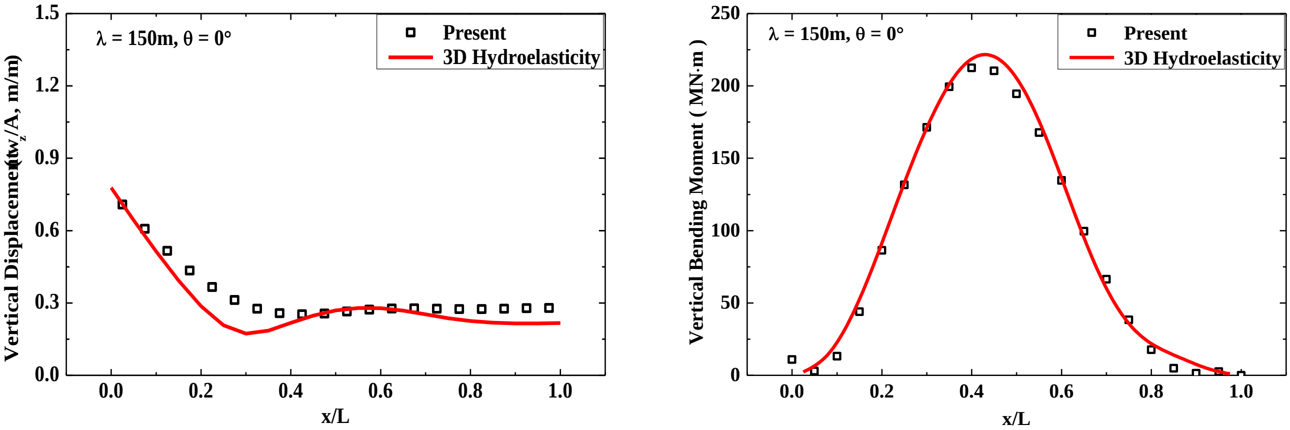

(a) Vertical displacement (b) Vertical bending moment

Fig. 15 Responses of a Wigley hull model

According to the verifications of the above two models, the proposed method is applicable to hydroelastic response analysis on any shape of floating structures for both finite and infinite water depths.

4. Hydroelasticity of floating structures in inhomogeneous conditions

4.1. Floating structures under an uneven sea bottom

Song et al. (2005) experimentally investigated the effects of an uneven sea bottom, including both

2D and 3D regular shoal bottoms, on the hydroelastic responses of a floating plate under regular waves. The parameters of the floating plate are listed in Table 4, and the model is discretized into 20 modules along the longitudinal direction after the convergence study. The 2D cylinder shoal bottom with an oval cross section in Song et al. (2005) is chosen as the uneven-bottom numerical example, as shown in

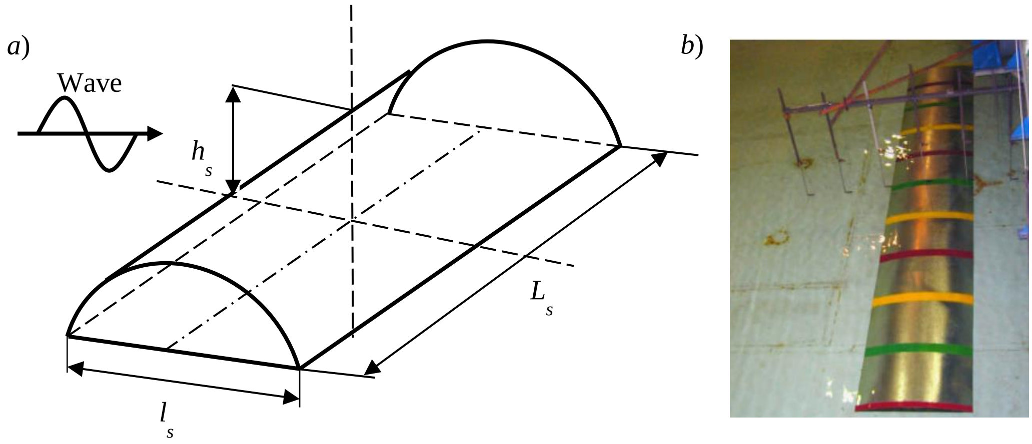

Fig. 16 and listed in Table 5. Fig. 17 illustrates the wetted surface panels of the shoal bottom and the floating plate, where the cylindrical bottom is modeled as a fixed body on the seabed and the floating plate is modeled as a normal flexible floating structure.

Table 4 Main parameters of the floating plate

Parameter	Length L (m)	Breadth B (m)	Draft d (m)	Vertical Bending Stiffness EI_y (N.m^2)
Designation	1000	60	1	1.11E12

Table 5 Dimension of the shoal model

Type	Length of section l_s (m)	Height of section h_s (m)	Length of cylinder L_s (m)
Two-dimensional	100	10	600

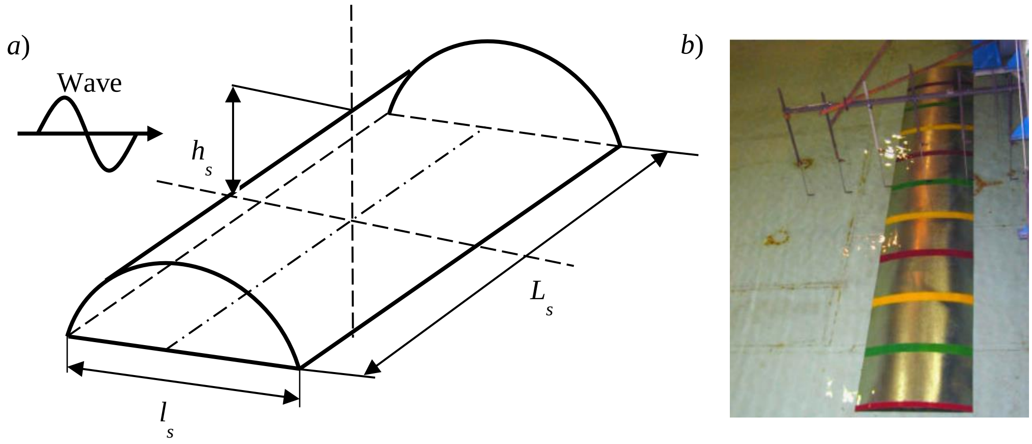

Fig. 16 Shoal model

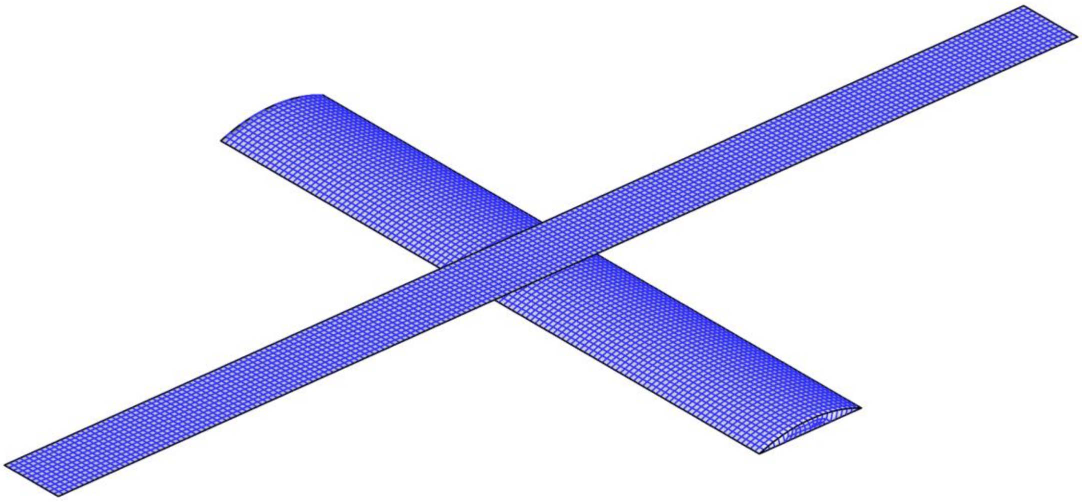

Fig. 17 Numerical model of a floating plate under an uneven bottom

Fig. 18 shows the corresponding numerical results from the proposed method and the experimental results by Song et al. (2005) for both flat-bottom and uneven-bottom conditions. This figure shows generally good agreements in terms of the vertical displacements. As seen from the figures, the effect of the non-uniform bottom on the vertical displacements along the longitudinal direction of the structure becomes stronger with increasing wavelength, especially around the location of the shoal arrangement. The non-uniformity has little effect if the water depth becomes larger because of small disturbances on the wave field. Meanwhile, some deviations are found between the proposed method and the experimental data, which may be caused by wave nonlinearity in shallow water and is not considered in the proposed method. As introduced by Mei et al. (1989), the nonlinearity of the waves could be quantified by the following

Ursell parameter:

$$U_r = \frac{A}{h}\frac{1}{(kh)^2} = \frac{A\lambda^2}{h^3(2\pi)^2} \tag{30}$$

where A is the wave amplitude; h is the water depth; k is the wave number, where $k = 2\pi/\lambda$; and λ is the wavelength.

Table 6 Value of U_r for different wavelengths and water depths

Water depth/ Wavelength	h=10 m	h=20 m	h=30 m	h=40 m
λ=100 m	0.25	0.032	0.009	0.004
λ=200 m	1.01	0.127	0.037	0.016
λ=400 m	4.05	0.507	0.151	0.063

According to wave dynamics, a wave is strongly nonlinear when $U_r \gg 1$, isolated or conoidal when $U_r = O(1)$, and linear with a small amplitude when $U_r \ll 1$. As shown in Table 6, the water depth is only 10 m on the top of the uneven sea bottom, and the Ursell parameters for wavelengths of 200 m and 400 m are beyond the scope of linear small-amplitude waves. For a wavelength of 200 m with *Ur*=1.01, the vertical displacements from the proposed method are slightly smaller than those from the model test around the uneven bottom. However, for a wavelength of 400 m with *Ur*=4.05, the proposed linear method, which cannot consider wave energy loss, exhibits larger vertical displacements compared to the experimental data.

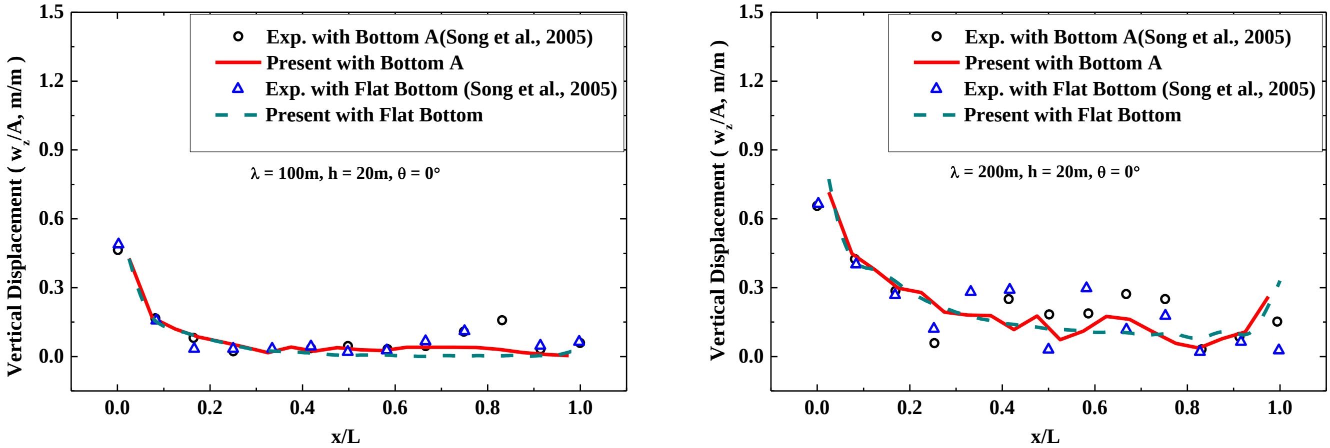

(a) λ=100m, $h = 20m$, θ=0° (b) λ=200m, $h = 20m$, θ=0°

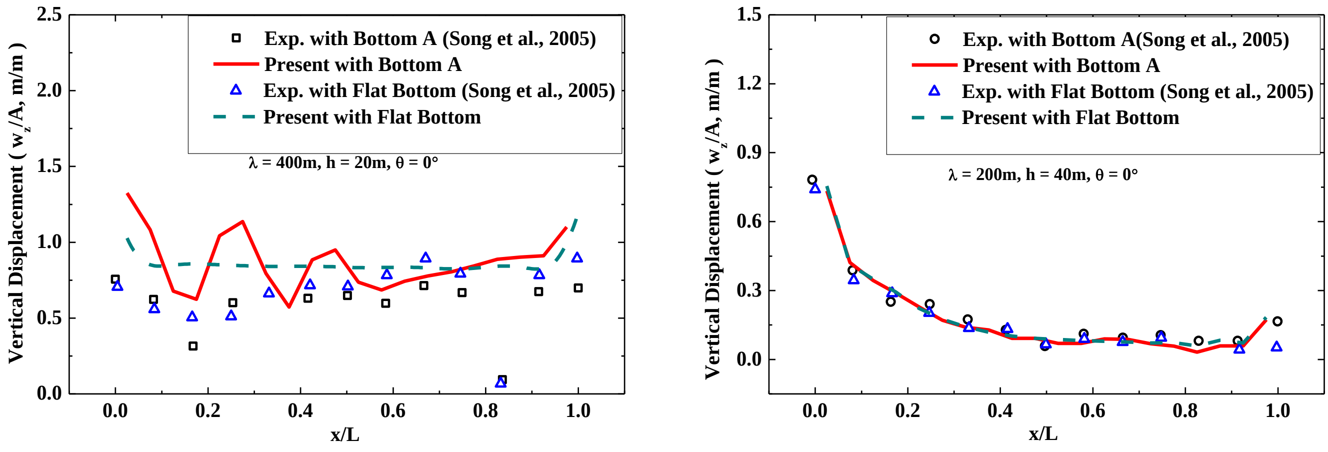

(c) λ=400m, $h=20m$, θ=0°   (d) λ=200m, $h=40m$, θ=0°

Fig. 18 Vertical displacement along the centerline on an uneven bottom

4.2. Hydroelastic responses of a floating plate in inhomogeneous waves

Waves are affected by islands and/or the shores of fjords when arriving from the open sea at certain angles or when passing by islands, and the wave field becomes inhomogeneous (Ding et al.; Lie et al., 2016). A typical inhomogeneous wave field that acts on a VLFS near an island is observed, with three sets of wave directions and wave spectra along the longitudinal region of the VLFS (Ding et al., 2016).

The hydroelastic responses of the floating plate (mode 1) in Table 1 for regular waves with different incident wave directions (wave height fixed at 2 m) are investigated to reveal the effects of inhomogeneity in the frequency domain as a numerical case. The floating structure is first discretized into 8 modules and then grouped into 3 regions with regular incident wave directions of 55 °, 90 °and 70 °, as shown in Fig. 19.

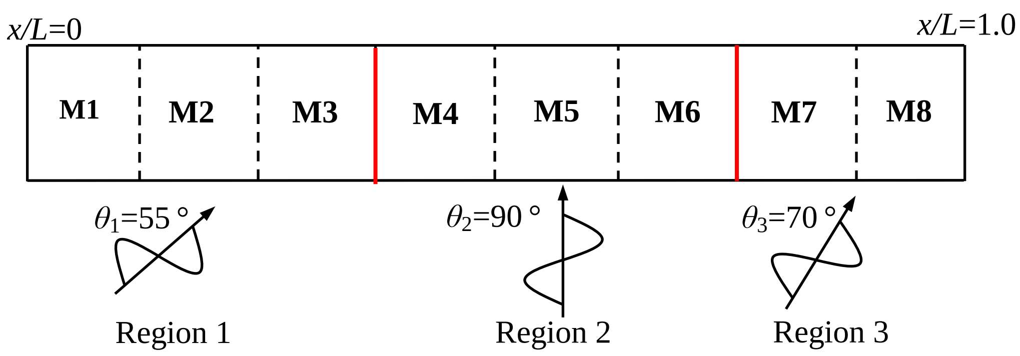

Fig. 19 Distribution diagram of the inhomogeneous regular wave conditions

The hydroelastic responses of the structure in each homogeneous regular wave component in the inhomogeneous wave are calculated and then compared to those in the inhomogeneous wave to determine the effects of the inhomogeneity of the incident waves.

As shown in Fig. 20, the difference in the vertical displacement at *x/L*=0.25 in inhomogeneous and homogeneous waves is not obvious. However, the vertical displacement at *x/L*=1.0 in the inhomogeneous wave is apparently different from those in homogeneous waves. Inhomogeneity induces a 20%~40% increase in the maximum vertical displacement compared to that in the most severe homogeneous wave condition (θ=55°), and the peak frequency decreases.

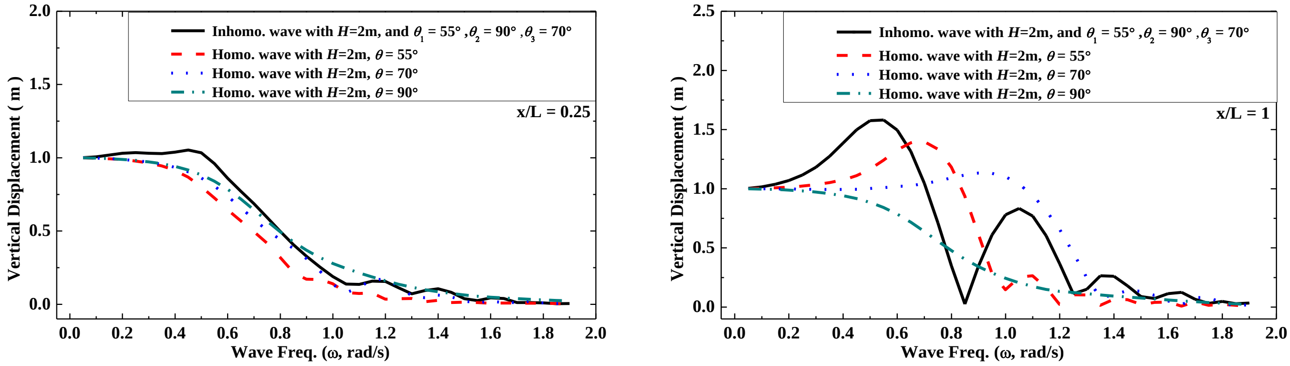

(a) Vertical displacement at *x/L*=0.25 (b) Vertical bending moment at *x/L*=1

Fig. 20 Vertical displacements in different positions along the structure in homogenous and inhomogeneous regular wave conditions.

Fig. 21 shows the distributions of the vertical bending moments and shear forces along the longitudinal direction of the structure at a wave frequency of 0.6rad/s in both homogeneous and inhomogeneous wave conditions. As shown in Fig. 21(a), the bending moments for homogeneous waves of 55° and 70° have two peaks around the positions of *x/L*=0.4 and 0.6, respectively, and are almost zero in beam seas (θ=90°). However, when the structure encounters inhomogeneous waves, the maximum bending moment along the longitudinal direction of the structure is almost double that of the result in the most severe homogeneous wave (θ=55°), and the position with the maximum bending moment moves from the middle to the waves from side. Similar trends can be also found in the distribution of the vertical shear forces, and the inhomogeneity of waves induces almost three times maximum bending moment, compared that in the most severe homogeneous wave (θ=55°), as shown in Fig. 21(b).

Moreover, the bending moments and shear forces at two typical positions, namely, *x/L*=0.2 and 0.5

for vertical bending moments and *x/L*=0.3 and 0.75 for shear forces, are investigated under different wave frequencies. As shown in Fig. 22, the maximum vertical bending moment at the position of *x/L*=0.2 in the inhomogeneous wave condition is obviously larger than that in homogeneous wave conditions, and the peak frequency for inhomogeneous waves moves to a lower wave frequency. However, the inhomogeneity at the position of *x/L*=0.5 does not cause significant differences in the maximum value of the bending moment. The same trends can be also found in the distributions of the shear forces.

Generally, in a specific wave frequency, the inhomogeneity of the regular wave may induce 2~3 times increase in the maximum bending moments/shear forces along the longitudinal structure, compared to homogeneous waves.

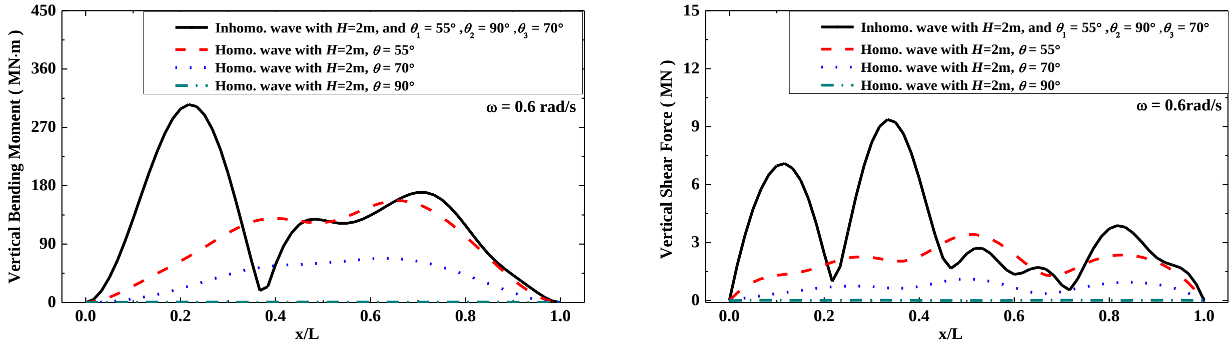

(a) Vertical bending moment for ω=0.6rad/s (b) Vertical shear force for ω=0.6rad/s

Fig. 21 Vertical bending moments and shear forces along the structure in homogenous and inhomogeneous regular wave conditions.

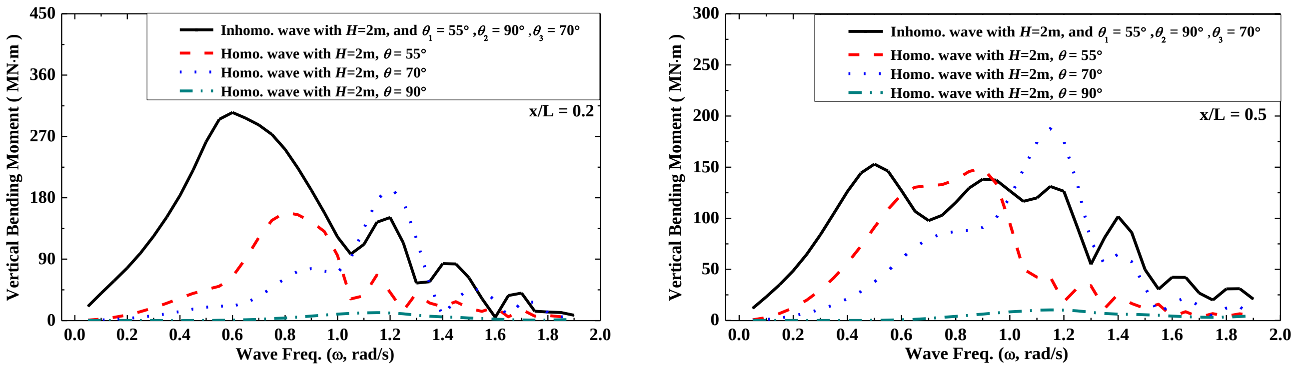

(a) Vertical bending moment at *x/L*=0.2 (b) Vertical bending moment at *x/L*=0.5

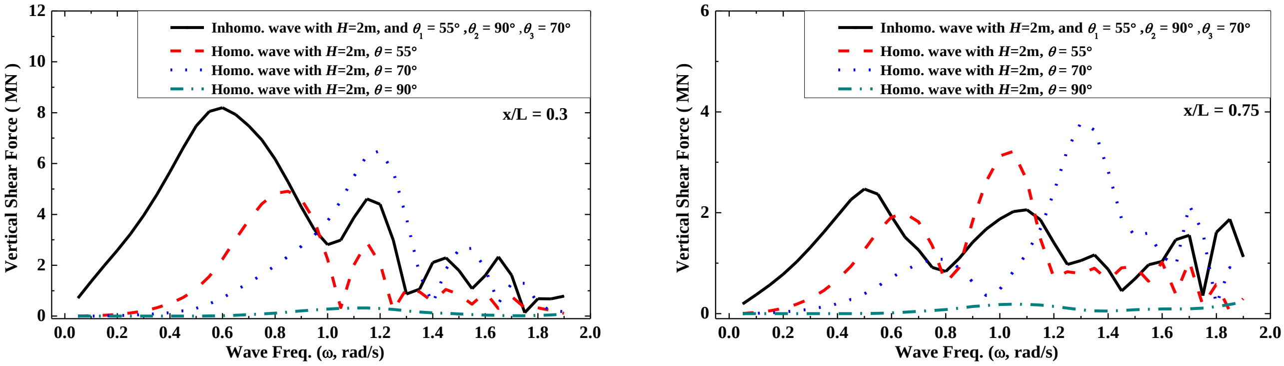

(c)Vertical shear force at *x/L*=0.3 (d) Vertical shear force at *x/L*=0.75

Fig. 22 Vertical bending moments and shear forces along wave frequencies in different positions in homogenous and inhomogeneous regular wave conditions.

5. Concluding remarks

A discrete-modules-based method was developed based on the three-dimensional potential theory and structural mechanics to investigate the hydroelastic behaviors of floating structures in both homogeneous and inhomogeneous seabed and wave field conditions. The following conclusions can be drawn:

1) The proposed method has been verified against the model tests and the conventional 3D hydroelastic method in homogeneous waves. Moreover, this method could directly evaluate the connecting forces for interconnected flexible floating structures.
2) The hydroelastic responses of a floating plate according to this method showed good agreement with published experimental data when considering an uneven sea bottom.
3) The inhomogeneity of regular waves could induce an approximately 30%~80% increase in the maximum bending moments/shear forces compared to homogeneous waves, which should be considered to achieve safe design.

Only inhomogeneous regular wave conditions with different incident wave directions were investigated in the frequency domain in this paper. The effects of inhomogeneous irregular wave conditions (different directions and spatial varying wave parameters) on the hydroelastic responses under real sea conditions will be considered and examined in future work.

Acknowledgments

This research was supported by the National Science Foundation of China (Grant No. 51490674) and the research project on high-technology ships supported by the Ministry of Industry and Information Technology. The insightful comments by the reviewers of this paper are highly appreciated.

Reference

Belibassakis, K., Athanassoulis, G., 2005. A coupled-mode model for the hydroelastic analysis of large floating bodies over variable bathymetry regions. J. Fluid Mech. 531, 221–249.

Betts, C., Bishop, R., Price, W., 1977. The symmetric generalised fluid forces applied to a ship in a seaway. RINA Suppl. Pap. 119.

Bishop, R., Price, W., Temarel, P., 1979. A unified dynamical analysis of antisymmetric ship response to waves.

Bishop, R.E.D., Price, W., Wu, Y., 1986. A general linear hydro elasticity theory of floating structures moving in a seaway. Philos. Trans. R. Soc. Lond. Ser. A Math. Phys. Eng. Sci. 316, 375–426.

Chen, X.-j., Wu, Y.-s., Cui, W.-c., Jensen, J.J., 2006. Review of hydroelasticity theories for global response of marine structures. Ocean Eng. 33, 439–457.

Ding, J., Tian, C., Wu, Y., Li, Z., Lu, Z., Wu, X., 2016. Hydroelasticity of a VLFS in non-uniform incident waves.

Ertekin, R.C., Kim, J.W., 1999. Hydroelastic response of a floating mat-type structure in oblique, shallow-water waves. J. Ship Res. 43, 241–254.

Fu, S., Moan, T., Chen, X., Cui, W., 2007. Hydroelastic analysis of flexible floating interconnected structures. Ocean Eng. 34, 1516–1531.

Gao, R., Tay, Z., Wang, C., Koh, C., 2011. Hydroelastic response of very large floating structure with a flexible line connection. Ocean Eng. 38, 1957–1966.

Gerostathis, T.P., Belibassakis, K., Athanassoulis, G., 2016. 3D hydroelastic analysis of very large floating bodies over variable bathymetry regions. J. Ocean Eng. Mar. Energy 2, 159–175.

Hu, J.-J., Wu, Y.-S., Tian, C., Wang, X.-L., Zhang, F., 2012. Hydroelastic analysis and model tests on the structural responses and fatigue behaviours of an ultra-large ore carrier in waves. Proc. Inst. Mech. Eng. M 226, 135–155.

Humamoto, T., Fujita, K., 2002. Wet-mode superposition for evaluating the hydroelastic response of floating structures with arbitrary shape. In: The Twelfth International Offshore and Polar Engineering Conference. International Society of Offshore and Polar Engineers.

Kim, B.W., Hong, S.Y., Kyoung, J.H., Cho, S.K., 2007. Evaluation of bending moments and shear forces at unit connections of very large floating structures using hydroelastic and rigid body analyses. Ocean Eng. 34, 1668–1679.

Kyoung, J.H., Hong, S.Y., Kim, B.W., Cho, S.K., 2005. Hydroelastic response of a very large floating structure over a variable bottom topography. Ocean Eng.32, 2040–2052.

Lee, K.-H., Cho, S., Kim, K.-T., Kim, J.-G., Lee, P.-S., 2015. Hydroelastic analysis of floating structures with liquid tanks and comparison with experimental tests. Appl. Ocean Res. 52, 167–187.

Lee, K.-H., Lee, P.-S., 2016. Nonlinear hydrostatic analysis of flexible floating structures. Appl. Ocean Res. 59, 165–182.

Lee, C.-H., Newman, J., 2000. An assessment of hydroelasticity for very large hinged vessels. J. Fluids Struct. 14, 957–970.

Lie, H., Fu, S., Fylling, I., Fredriksen, A.G., Bonnemaire, B., Kjersem, G.L., 2016. Numerical modelling of floating and submerged bridges subjected to wave, current and wind. In: ASME 2016 35th International Conference on Ocean, Offshore and Arctic Engineering. American Society of Mechanical Engineers, V007T006A075.

Loukogeorgaki, E., Michailides, C., Angelides, D.C., 2012. Hydroelastic analysis of a flexible mat-shaped floating breakwater under oblique wave action. J. Fluids Struct. 31, 103–124.

Lu, D., Fu, S., Zhang, X.F., Guo, Y., 2016. A method to estimate the hydroelastic behaviour of VLFS based on multi-rigid-body dynamics and beam bending. Ships and Offshore Struct 1–9.

Malenica, S., Tuitman, J., 2008. 3DFEM-3DBEM model for springing and whipping analyses of ships. In: RINA conference, London.

Mei, C.C., Stiassnie, M., Yue, D.K.-P., 1989. Theory and Applications of Ocean Surface Waves: Part 1: Linear Aspects Part 2: Nonlinear Aspects. World Scientific.

Michailides, C., Loukogeorgaki, E., Angelides, D.C., 2013. Response analysis and optimum configuration of a modular floating structure with flexible connectors. Appl. Ocean Res. 43, 112–130.

Murai, M., Inoue, Y., Nakamura, T., 2003. The prediction method of hydroelastic response of VLFS with sea bottom topographical effects. In: The Thirteenth International Offshore and Polar Engineering Conference. International Society of Offshore and Polar Engineers.

Newman, J., 2005. Efficient hydrodynamic analysis of very large floating structures. Mar.

Struct.18, 169–180.
Ohkusu, M., Namba, Y., 2004. Hydroelastic analysis of a large floating structure. J. Fluids Struct.19, 543–555.
Senjanović, I., Malenica, Š., Tomas, S., 2008a. Investigation of ship hydroelasticity. Ocean Eng. 35, 523–535.
Senjanović, I., Tomić, M., Tomašević, S., 2008b. An explicit formulation for restoring stiffness and its performance in ship hydroelasticity. Ocean Eng. 35, 1322–1338.
Shin, K.-H., Jo, J.-W., Hirdaris, S.E., Jeong, S.-G., Park, J.B., Lin, F., Wang, Z., White, N., 2015. Two-and three-dimensional springing analysis of a 16,000 TEU container ship in regular waves. Ships Offshore Struct. 10, 498–509.
Song, H., Tao, L., Cui, W., Liu, Y., 2005. Hydroelastic response of VLFS on Uneven Sea bottom. In: ASME 2005 24th International Conference on Offshore Mechanics and Arctic Engineering. American Society of Mechanical Engineers, pp. 433–443.
Taghipour, R., Perez, T., Moan, T., 2009. Time-domain hydroelastic analysis of a flexible marine structure using state-space models. J. Offshore Mech. Arct. Eng. 131, 011603.
Utsunomiya, T., Watanabe, E., Nakamura, N., 2001. Analysis of drift force on VLFS by the near-field approach. In: The Eleventh International Offshore and Polar Engineering Conference. International Society of Offshore and Polar Engineers.
Wu, Y, 1984. Hydroelasticity of Floating Bodies. University of Brunel.
Wu, Y., Maeda, H., Kinoshita, T., 1997. The second order hydrodynamic actions on a flexible body. J. Inst. Ind. Sci. Univ. Tokyo 49, 8–19.
Xia, D., Kim, J.W., Ertekin, R.C., 1999. The effect of shoreline proximity on the hydroelastic response of a floating runway. In: Proceedings of the 18th International Conference on Offshore Mechanics and Arctic Engineering (OMAE'99), St. John'S, Newfoundland, Canada. American Society of Mechanical Engineers, New York, p. 8.
Xia, J., Wang, Z., Jensen, J.J., 1998. Non-linear wave loads and ship responses by a time-domain strip theory. Mar. Struct. 11, 101–123.
Yago, K., Endo, H., 1996. On the hydoroelastic response of box-shaped floating structure with shallow draft. J. Soc. Naval Arch. Japan 1996, 341–352.
Yoon, J.-S., Cho, S.-P., Jiwinangun, R.G., Lee, P.-S., 2014. Hydroelastic analysis of floating plates

with multiple hinge connections in regular waves. Mar. Struct. 36, 65–87.